

Grain size segregation during bedload transport on steep slopes

Rémi Chassagne¹†, Raphaël Maurin³, Julien Chauchat², J. M. N. T. Gray⁴ and Philippe Frey¹

¹Univ. Grenoble Alpes, Irstea, UR ETNA, 38000 Grenoble, France

²Univ. Grenoble Alpes, LEGI, CNRS UMR 5519 - Grenoble, France

³IMFT, Univ. Toulouse, CNRS - Toulouse, France

⁴Department of Mathematics, University of Manchester, Manchester M13 9PL, UK

(Received xx; revised xx; accepted xx)

Size segregation in bedload transport is studied numerically with a coupled fluid-discrete element model. Starting from an initial deposit of small spherical particles on top of a large particle bed, the segregation dynamics of the bed is studied as it is driven by the fluid flow. Focusing on the quasi-static part of the bed, the small particles are observed to segregate as a layer of constant thickness at a velocity constant in time and independent of the number of small particles. The segregation velocity is observed to be directly linked to the inertial number at the bottom of the layer, and to increase linearly with the size ratio. While the macroscopic behavior is independent of the concentration in small particles, an analysis in the framework of the continuous model of Thornton *et al.* (2006) shows that the dynamics results from an equilibrium between the influence of the local concentration and the inertial number forcing. Deriving an analytical solution of the continuous model, it is shown that the diffusion coefficient should have the same dependency on the inertial number as the segregation flux. Implementing the segregation and the diffusive fluxes in the continuous model, it is shown that they quantitatively reproduce the discrete simulations. These results improve the understanding of the size segregation dynamics and represent a step forward in the upscaling process of polydisperse granular flow in the context of turbulent bedload transport.

1. Introduction

Bedload transport, the coarser sediment load transported by a flowing fluid in contact with the mobile stream bed by rolling, sliding and/or saltating, has major consequences for public safety, water resources and environmental sustainability. In mountains, steep slopes drive an intense transport of a wide range of grain sizes implying size sorting or segregation, which is largely responsible for our limited ability to predict sediment flux and river morphology (Bathurst 2007; Frey & Church 2011; Dudill *et al.* 2018).

The present study focuses on size segregation. For large size ratios, the small particles can percolate without external forcing by gravity into the bed of larger particles (Bridgwater & Ingram 1971; Dudill *et al.* 2017). For the smaller size ratios, percolation is not possible without deformation of the bed, which can be achieved by shearing or vibrating. This dynamic segregation results from the combination of kinetic sieving (Middleton 1970) and squeeze expulsion (Savage & Lun 1988). Kinetic sieving is based on the idea that, when sheared, granular media experience velocity fluctuations creating holes between particles, in which small particles are more probable to fall into than

† Email address for correspondence: remi.chassagne@irstea.fr

large particles. In opposition, squeeze expulsion tends to push all particles upwards with the same probability. The combination of both processes, which for brevity will just be called kinetic sieving in the following, results in a net flux downward for the small particles and upward for the large, leading to an inverse graded bed. Kinetic sieving has then been studied experimentally and numerically in multiple configurations such as dry granular avalanches (Savage & Lun 1988; Dolgunin & Ukolov 1995; Wiederseiner *et al.* 2011; Fan *et al.* 2014; Jones *et al.* 2018), shear cells (Golick & Daniels 2009; May *et al.* 2010; Van der Vaart *et al.* 2015; Fry *et al.* 2018), annular rotating drum (Gray & Ancey 2011) and laminar bedload configurations (Ferdowski *et al.* 2017).

In order to identify the mechanisms and comment on the literature on kinetic sieving, a dimensional analysis is performed. This analysis is made in the dry limit case, consistent with the results of Maurin *et al.* (2016) showing that the fluid just acts as a forcing mechanism in turbulent bedload transport. The different parameters of the problem are

$$d_s, d_l, \phi_s, \rho^p, g, \dot{\gamma}^p, P, w_s, \quad (1.1)$$

where d_s (resp. d_l) is the diameter of small (resp. large) particles, ϕ_s is the local concentration in small particles, ρ^p is the particle density, $g = 9.81 \text{ m s}^{-2}$ is the gravity acceleration, $\dot{\gamma}^p$ is the particle shear rate, P is the granular pressure and w_s is the segregation velocity of the small particles. These eight variables involve only three units (length, time and mass), so the problem depends on five dimensionless parameters. Choosing d_l , $\sqrt{d_l/g}$ and $\rho^p d_l^3$ as reference length, time and mass units respectively, the following relation is obtained

$$\frac{w_s}{\sqrt{g d_l}} = \mathcal{G} \left(r, \phi_s, \sqrt{\frac{d_l}{g}} \dot{\gamma}^p, \frac{P}{\rho^p d_l g} \right), \quad (1.2)$$

where $r = d_l/d_s$ is the size ratio between large and small particles and \mathcal{G} is an unknown function. It is assumed that relation (1.2) can be written in a power law form,

$$\frac{w_s}{\sqrt{g d_l}} \propto (r - 1)^l \left(\sqrt{\frac{d_l}{g}} \dot{\gamma}^p \right)^m \left(\frac{P}{\rho^p d_l g} \right)^n \mathcal{G}_1(\phi_s), \quad (1.3)$$

where the dependence on the size ratio has been written as $(r - 1)^l$ in order to cancel segregation in the monodisperse limit.

In the theory of Savage & Lun (1988), $\dot{\gamma}^p$ is predicted to be a controlling parameter for size segregation as the shear rate allows particles to move relatively faster than the one below them and find holes in which to segregate. With experiments of bidisperse flows down inclined planes, Savage & Lun (1988) measured concentration profiles at different streamwise positions and found good agreement between the theory and experiments. With discrete element method (DEM) simulations of dry bidisperse mixtures in a heap flow configuration, Fan *et al.* (2014) measured the percolation velocity of each species and found a linear relation between the percolation velocity and the shear rate. In a shear cell experiment with a rotating bottom plate and a weighted top plate, Golick & Daniels (2009) evidenced the effect of pressure on segregation. Small particles were initially placed above large particles, and they characterized the segregation rate by measuring the volume evolution of the cell. They found that the segregation rate slows down strongly with granular pressure. In a dry confined shear cell, Fry *et al.* (2018) also observed this effect of pressure on segregation and found a power law relating

the segregation rate and the inertial number I (GDR MiDi 2004). The latter scaling represents an extension of the Savage & Lun (1988) theory in order to take into account both the effect of the shear rate and pressure on segregation. It corresponds in (1.3) to $n = -m/2$, which can be rewritten as

$$\frac{w_s}{\sqrt{gd_l}} \propto (r-1)^l I^m \mathcal{G}_1(\phi_s), \quad (1.4)$$

with I the large particle inertial number defined as

$$I = \frac{d_l \dot{\gamma}^p}{\sqrt{P/\rho^p}} \quad (1.5)$$

suggesting that the segregation velocity is a function of the inertial number, the size ratio and the local concentration.

The size ratio between large and small particles r is also a key parameter for size segregation. Smaller particles are expected to segregate more easily. In the annular cell configuration, Golick & Daniels (2009) showed that the segregation rate is an increasing function of the size ratio with a maximum around $r = 2$. In 2D DEM simulations of sheared and confined granular flow, Guillard *et al.* (2016) measured the segregation force applied on a single large particle placed in a small particle mixture. They also showed that the segregation force increases with r and observed the same maximum around $r = 2$.

The effect of the small particle concentration ϕ_s has also been widely studied, and different forms for \mathcal{G}_1 have been proposed (Bridgwater *et al.* 1985; Savage & Lun 1988; Dolgunin & Ukolov 1995; Gray & Thornton 2005; May *et al.* 2010; Gajjar & Gray 2014; Van der Vaart *et al.* 2015; Fan *et al.* 2014). The small particles have been shown to segregate less easily if they are more concentrated and the downward velocity should vanish for a pure phase of small particles. For this purpose, the simplest form $\mathcal{G}_1(\phi_s) = 1 - \phi_s$, has been proposed by Dolgunin & Ukolov (1995). In oscillating cell experiments, Van der Vaart *et al.* (2015) measured the time necessary to achieve complete segregation with an initial mixture ranging from one small particle falling into a bed of large particles to a unique large particle going up in a small particle bed. They observed that both extreme cases were not symmetric, resulting in an asymmetry of the vertical velocity with the concentration and Gajjar & Gray (2014) proposed thereby a quadratic form for \mathcal{G}_1 with ϕ_s . Simulations by Fan *et al.* (2014); Jones *et al.* (2018) of dry bidisperse avalanches, observed this non linearity of the velocity when ϕ_s is close to zero, but concluded that the form of Dolgunin & Ukolov (1995) is at first order a good approximation.

The literature review on dry granular flows underlines the qualitative understanding of size-segregation for simple flows. Bedload transport can be seen as a granular flow, where the coupling with the fluid induces strong gradients in the vertical direction and a complex forcing, which could challenge the classical picture of segregation. Few studies have been made on kinetic sieving in bedload transport and more remains to be done for a clear understanding of the processes at play. Ferdowsi *et al.* (2017) studied experimentally size segregation in laminar bedload transport and performed dry granular flow simulations. They studied the formation of armour, i.e. the segregation of large particles to the top, starting from a mixture of small and large particles. They showed that the process seems to be a granular phenomenon and reproduced their experimental results in the framework of continuous segregation modelling, using an ad-hoc parametrisation of the model. Hergault *et al.* (2010) and Frey *et al.* (2019)

studied size-segregation in turbulent bedload transport, considering a quasi-2D channel enabling particle tracking. They found that the particles move down as a layer into the bed, and related the segregation velocity to the granular shear rate.

Modelling turbulent bedload transport segregation phenomenon at the particle scale is computationally demanding and can be only achieved for very small domains. In this context, one of the main goals for segregation in turbulent bedload transport is to be able to do upscaling to the framework of continuous modelling. In this case, it includes the modelling of the fluid phase, the granular phase and the evolution of the different classes of particles with respect to one another. Such a segregation model has been developed by Gray & Thornton (2005), Thornton *et al.* (2006) and Gray & Chugunov (2006). This three phase model is based on the assumption that the overburden granular pressure is not shared equally between large and small particles (Gray & Thornton 2005). Substituting this into the momentum conservation equation of each constituent and placing the problem within the framework of the mixture theory, an evolution equation for the phase of small particles is found

$$\frac{\partial \phi_s}{\partial t} + \nabla \cdot (\phi_s \mathbf{u}) - \frac{\partial F_s}{\partial z} = \nabla \cdot (D \nabla \phi_s), \quad (1.6)$$

where \mathbf{u} is the bulk velocity field, D the diffusion coefficient, F_s the segregation flux. The physics relies on the expression of the segregation flux and of the diffusion flux. The former is defined as $F_s = \phi_s w_s$ and can therefore directly be linked to the above stated results. Introducing the dimensional analysis (1.4) and considering the simplest form of Dolgunin & Ukolov (1995) for \mathcal{G}_1 the following segregation flux is obtained

$$F_s \propto (r - 1)^l I^m \phi_s (1 - \phi_s). \quad (1.7)$$

In granular flows, diffusion has been mainly studied in the case of self-diffusion. By analogy to the thermal diffusion of molecules, Campbell (1997) tracked, in numerical simulations of dilute monodisperse sheared flows, the random motions of particles and showed that the diffusion coefficient should scale with the shear rate. In dense granular flows, Utter & Behringer (2004) also observed, in 2D Couette flow experiments, the dependency of the diffusion coefficient with the shear rate. The diffusion mechanism considered in this paper is the mixing of one class of particles into another. This kind of diffusion is expected to be related to self-diffusion, but to the best of our knowledge, no study has been done in order to determine the physical mechanism controlling this diffusion.

While the literature review underlined the progress in the understanding and modelling of kinetic sieving, more physically-based parametrisations of the continuous model are still lacking, in particular in the complex turbulent bedload transport configuration. In the present contribution, size segregation in turbulent bedload transport is studied numerically considering fluid-DEM simulations. The aim is to understand size segregation in the quasi-static part of the flow and to improve the continuous modelling parametrisations. In particular the influence of the three parameters r , I and ϕ_s and the values of exponents l and m , will be investigated through numerical experiments in the bedload configuration.

After presenting the numerical model (§ 2), numerical simulations of turbulent bedload transport will be presented and analysed based on the different expected dependencies from the dimensional analysis (§ 3). The results are then studied, through an analytical analysis, in the framework of continuous modelling and highlight the local segregation

mechanisms. This analysis shows that diffusion and segregation should have the same dependence on the inertial number and enables quantitatively reproducing the DEM results (§ 4).

2. Fluid-DEM model for bidisperse system

The numerical model used to simulate size-segregation in turbulent bedload transport is a three-dimensional Discrete Element Method (DEM) using the open-source code YADE (Smilauer et al. 2015) coupled with a vertical one-dimensional turbulent fluid model. This code has been validated with particle-scale experiments (Frey 2014) in Maurin *et al.* (2015) for mono-disperse situations. A brief summary of the model formulation as well as a description of its adaptation to bi-disperse situations is now given.

2.1. Granular phase

DEM is a Lagrangian method based on the resolution of contacts between particles. For each spherical particle p , the motion of the particle is obtained from Newton's second law, and a momentum equation and an angular momentum conservation equation are solved

$$m^p \frac{d^2 \mathbf{x}^p}{dt^2} = \mathbf{f}_g^p + \mathbf{f}_c^p + \mathbf{f}_f^p, \quad (2.1)$$

$$\mathcal{I}^p \frac{d\boldsymbol{\omega}^p}{dt} = \boldsymbol{\tau} = \mathbf{x}_c \times \mathbf{f}_c^p, \quad (2.2)$$

where m^p , \mathbf{x}^p , $\boldsymbol{\omega}^p$ and \mathcal{I}^p are respectively the mass, position, angular momentum and moment of inertia of particle p . The three major forces are: \mathbf{f}_g^p the gravitational force, \mathbf{f}_c^p the inter-particles contact forces and \mathbf{f}_f^p the interaction forces with the fluid. The inter-particles contact forces are classically defined as a spring-dashpot system (Schwager & Poschel 2007) composed of a spring of stiffness k_n in parallel with a viscous damper of coefficient c_n in the normal direction; and a spring of stiffness k_s associated with a slider of friction coefficient μ in the tangential direction. The normal and tangential contact forces reads accordingly

$$\begin{aligned} F_n &= -k_n \delta_n - c_n \dot{\delta}_n, \\ F_t &= -\min(k_s \delta_t, \mu_p F_n), \end{aligned} \quad (2.3)$$

where δ_n (resp. δ_t) is the overlap between particles in the normal (resp. tangential) direction. For each class of particles, the value of k_n and k_s are computed in order to stay in the rigid limit of grains (Roux & Combe 2002; Maurin *et al.* 2015). The normal stiffness in parallel with the viscous damper, defines a restitution coefficient representative of the loss of energy during collisions, which is fixed to $e_n = 0.5$ for each contact. Finally the friction coefficient is fixed to $\mu = \arctan(0.4)$ for all particles independently of their diameter.

The third type of forces concerns the interactions with the fluid which are restricted in this model to the buoyancy force and the drag force (Maurin *et al.* 2015). They are defined as:

$$\mathbf{f}_b^p = -\frac{\pi d^{p3}}{6} \nabla P^f, \quad (2.4)$$

$$\mathbf{f}_D^p = \frac{1}{2} \rho^f \frac{\pi d^{p2}}{4} C_D \|\langle \mathbf{u} \rangle_{\mathbf{x}^p}^f - \mathbf{v}^p\| \left(\langle \mathbf{u} \rangle_{\mathbf{x}^p}^f - \mathbf{v}^p \right), \quad (2.5)$$

where d^p denotes the diameter of particle p , $\langle \mathbf{u} \rangle_{\mathbf{x}^p}^f$ is the mean fluid velocity at the position of particle p and \mathbf{v}^p is the velocity of particle p . The drag coefficient takes into

account hindrance effects (Richardson & Zaki 1954) as $C_D = (0.4 + 24.4/Re_p)(1 - \Phi)^{-3.1}$, with Φ the total solid phase (small and large particles) volume fraction and $Re_p = \|\langle \mathbf{u} \rangle_{\mathbf{x}^p}^f - \mathbf{v}^p\| d^p / \nu^f$ the particle Reynolds number.

2.2. Fluid model

The fluid model is a one dimensional vertical turbulent model inspired from the Euler-Euler model proposed by Chauchat (2018) and solves directly the volume-averaged momentum balance for the fluid phase,

$$\rho^f (1 - \Phi) \frac{\partial \langle u_x \rangle^f}{\partial t} = \frac{\partial S_{xz}}{\partial z} - \frac{\partial R_{xz}}{\partial z} + \rho^f (1 - \Phi) g_x - n \langle f_{f_x}^p \rangle^s, \quad (2.6)$$

where ρ^f is the density of the fluid, S_{xz} is the effective fluid viscous shear stress of a Newtonian fluid, R_{xz} is the turbulent fluid shear stress and $n \langle f_{f_x}^p \rangle^s$ represents the momentum transfer associated with the interaction forces between fluid and particles.

The viscous shear stress S_{xz} is taken as

$$S_{xz} = \rho^f (1 - \Phi) \nu^f \frac{\partial \langle u_x \rangle^f}{\partial z}, \quad (2.7)$$

with ν^f the pure fluid viscosity. The Reynolds shear stress R_{xz} is based on an eddy viscosity concept,

$$R_{xz} = \rho^f (1 - \Phi) \nu_t \frac{\partial \langle u_x \rangle^f}{\partial z}. \quad (2.8)$$

The turbulent viscosity ν_t follows a mixing length approach that depends on the integral of the solid volume fraction profile to account for the presence of particles (Li & Sawamoto 1995),

$$\nu_t = l_m^2 \left| \frac{\partial \langle u_x \rangle^f}{\partial z} \right|, \quad l_m(z) = \kappa \int_0^z \frac{\Phi_{max} - \Phi(\zeta)}{\Phi_{max}} d\zeta, \quad (2.9)$$

with $\kappa = 0.41$ the Von-Karman constant and $\Phi_{max} = 0.61$ the maximal packing of the granular medium (random close packing).

The total momentum $n \langle f_{f_x}^p \rangle^s$ transmitted by the fluid to the particles is computed as the sum over each class of the horizontal solid-phase average (denoted $\langle \cdot \rangle^s$) of the momentum transmitted by the drag force to each particle :

$$n \langle f_{f_x}^p \rangle^s = \frac{\Phi_s}{\pi d_s^3 / 6} \langle f_{f_x}^{p_s} \rangle^s + \frac{\Phi_l}{\pi d_l^3 / 6} \langle f_{f_x}^{p_l} \rangle^s, \quad (2.10)$$

and introducing the expression of the drag force (2.5),

$$\begin{aligned} n \langle f_{f_x}^p \rangle^s &= \frac{3 \Phi_s \rho^f}{4 d_s} \left\langle C_D \|\langle \mathbf{u} \rangle_{\mathbf{x}^{p_s}}^f - \mathbf{v}^{p_s}\| \left(\langle \mathbf{u} \rangle_{\mathbf{x}^{p_s}}^f - \mathbf{v}^{p_s} \right) \right\rangle^s \\ &\quad + \frac{3 \Phi_l \rho^f}{4 d_l} \left\langle C_D \|\langle \mathbf{u} \rangle_{\mathbf{x}^{p_l}}^f - \mathbf{v}^{p_l}\| \left(\langle \mathbf{u} \rangle_{\mathbf{x}^{p_l}}^f - \mathbf{v}^{p_l} \right) \right\rangle^s, \end{aligned} \quad (2.11)$$

where p_s (resp. p_l) denotes the ensemble of the small (resp. large) particles, Φ_s (resp. Φ_l) the volume fraction of small (resp. large) particles, d_s (resp. d_l) the diameter of small (resp. large) particles.

The solid phase volume average $\langle \cdot \rangle^s$ is defined following Jackson (2000) for which a cuboid weighting function \mathcal{G} with the same length and width as the 3D domain is applied. In the vertical direction, in order to capture the strong vertical gradient of the

mean flow, the vertical thickness l_z of the box is chosen as $l_z = d_s/30$. This choice of weighting function has been validated by comparison with mono-disperse turbulent bedload transport experiments in Maurin *et al.* (2015). Therefore the mean values at position z are computed as

$$\Phi_s(z) = \sum_{p_s} \int_{V_{p_s}} \mathcal{G}(|z - z'|) dz', \quad (2.12)$$

$$\Phi_l(z) = \sum_{p_l} \int_{V_{p_l}} \mathcal{G}(|z - z'|) dz', \quad (2.13)$$

$$\langle \gamma \rangle^s = \frac{1}{\Phi_s(z)} \sum_{p_s} \int_{V_{p_s}} \gamma(z') \mathcal{G}(|z - z'|) dz' + \frac{1}{\Phi_l(z)} \sum_{p_l} \int_{V_{p_l}} \gamma(z') \mathcal{G}(|z - z'|) dz', \quad (2.14)$$

where γ is a scalar quantity.

In this paper, this model is used for a bi-disperse situation to study size segregation in bedload sediment transport.

3. DEM simulations of segregation dynamics

In this section, the infiltration of fine particles into the bed made of larger particles is studied during turbulent bedload transport using the numerical model described in the previous section.

3.1. Numerical setup

The numerical setup is presented in figure 1a. In the following, subscripts l and s denote quantities for large and small particles respectively. Initially, large particles of diameter $d_l = 6$ mm and fine particles of diameter $d_s = 4$ mm (size ratio $r = 1.5$) are deposited by gravity over a rough fixed bed made of large particles. The size of the 3D domain is $30d_l \times 30d_l$ in the horizontal plane in order to have converged average values (Maurin *et al.* 2015) and is periodic in the streamwise and spanwise directions. The number of particles of each class is assimilated to a number of layers, N_l and N_s . It represents in term of particle diameters the height that would be occupied by the particles if the packing fraction was exactly 0.61. The height of the bed at rest is thus defined by $H = N_l d_l + N_s d_s$ and H is fixed to $10d_l$ in all the simulations. The number of layers of fine particles N_s varies from 0.01 (only a few small particles) up to 2 layers (corresponding to figure 1a), while N_l changes accordingly in order to keep $H = 10d_l$. The bed slope is fixed to 10% (5.7°), representative of mountain streams. The Shields number is defined as the dimensionless fluid bed shear stress $\theta = \tau_f / [(\rho^p - \rho^f) g d_l]$ and simulations are performed at $\theta \simeq 0.1$. For this purpose, the free surface position is fixed and corresponds to a water depth of $h = 3.1d_l$.

At the beginning of each simulation, the fluid flows by gravity and sets particles into motion. A first transient phase takes place, during which fluid and particles are accelerating. During this period, segregation is very fast and at the end of the transient phase, the small particles have already infiltrated into the first layers of the bed. In this paper, the study focuses on the dynamics of segregation once the system is at transport equilibrium and small particles have reached the quasi-static layer.

The horizontal averaged volume fraction per unit granular volume of small (resp. large) particles is defined as ϕ_s (resp. ϕ_l). By definition, the two volume fractions sum to unity,

$$\phi_s + \phi_l = \frac{\Phi_s}{\Phi_s + \Phi_l} + \frac{\Phi_l}{\Phi_s + \Phi_l} = 1, \quad (3.1)$$

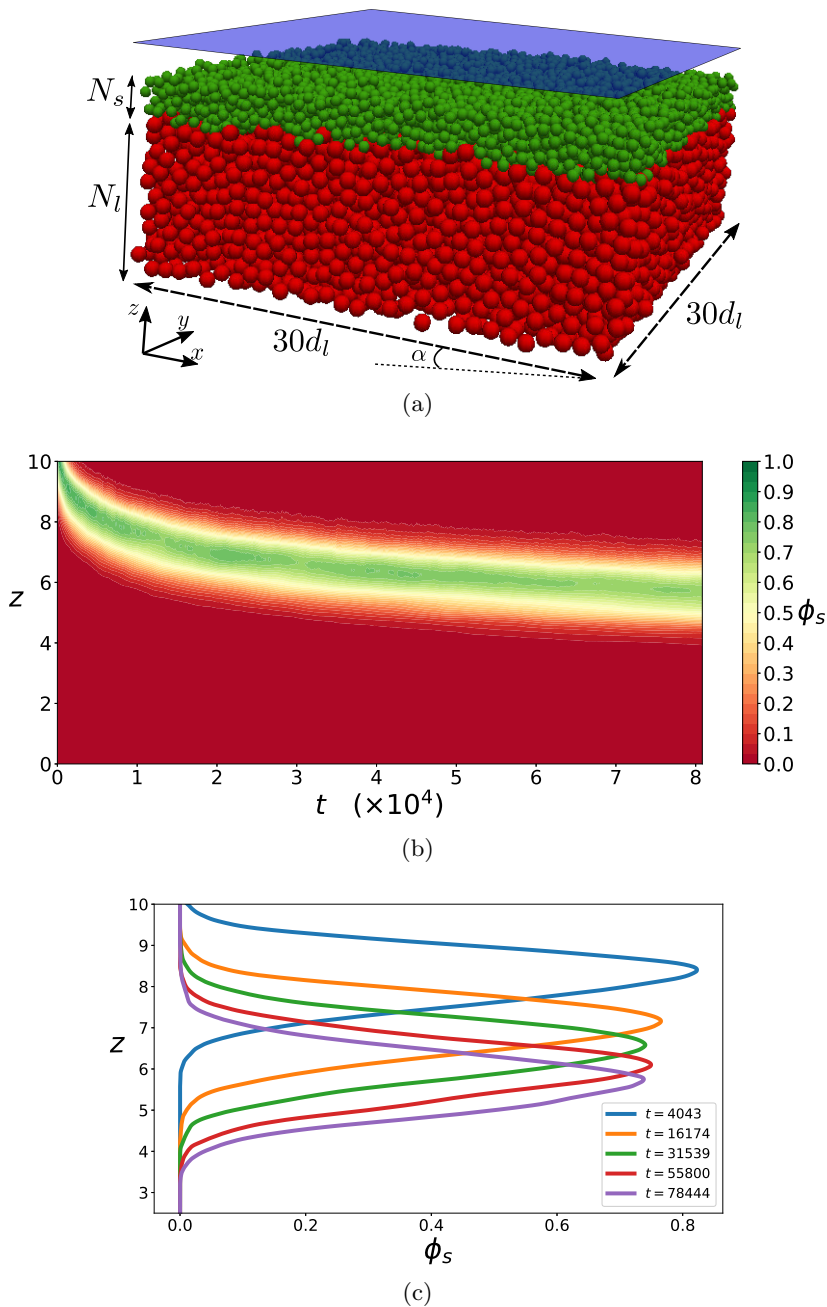


Figure 1: (a) Numerical setup, (b) Typical temporal evolution of fine particles concentration profile ϕ_s for the case $N_s = 2$, (c) Concentration profiles in small particles for different times.

where Φ_s (resp. Φ_l) is the volume the volume fraction of small (resp. large) particles defined per unit mixture volume as in the previous section. Lastly, z_c is defined as the vertical position of the center of mass of small particles and dz_c/dt as its velocity.

The results are presented without dimension and the following dimensionless variables

are considered,

$$\tilde{z} = \frac{z}{d_l}, \quad \tilde{t} = t\sqrt{g/d_l}, \quad \widetilde{\langle v_x \rangle^p} = \frac{\langle v_x \rangle^p}{\sqrt{gd_l}}. \quad (3.2)$$

In the following, the tildes are dropped for sake of clarity.

3.2. Results

Simulations have been performed for different numbers of layers of small particles N_s . Figure 1b shows the temporal evolution of fine particle concentration profiles for the case $N_s = 2$, corresponding to two layers of small particles deposited on top of a layer made of large particles. At the beginning, the small particles infiltrate rapidly into the first few layers of large particles. As small particles infiltrate downward, large particles rise to the surface. The DEM simulations exhibit a two layer structure, with small particles sandwiched between two layers of large particles. While infiltrating, the thickness of the small particle layer gets slightly larger. Profiles of concentration for different times are presented on figure 1c. The concentration profiles exhibit a Gaussian-like shape. After the transient phase, neither the maximal value nor the width of the profiles evolve in time, suggesting that the small particles infiltrate the bed as a layer having a constant thickness and that this layer is just convected downward by segregation inside the layer of large particles.

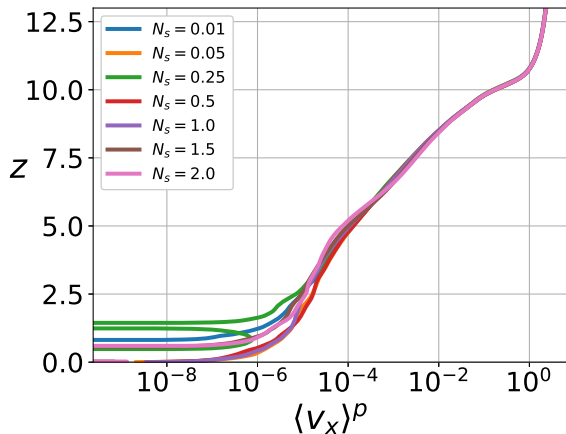
The vertical time and volume-averaged streamwise velocity profile of the particle mixture is plotted in figure 2a for all the simulations. All the curves are superimposed meaning that the response of the granular medium to the fluid flow forcing is not modified by the number of small particles. The granular forcing is therefore the same for all the simulations independently of the number of small particles in the initial condition. In the quasi-static region (i.e. between $z = 3$ and 8 approximately), the linearity of the profiles in the semilog plot indicates that the velocity is exponentially decreasing in the bed. Due to the presence of a fixed layer of particles at the bottom of the domain, the velocity goes to zero there. It is interesting to note that the entire bed is in motion, even if the velocity can be very low at the bottom of the quasi-static region. This is characteristic of a creeping flow.

Since the small particles infiltrate the bed as a layer, the center of mass of the small particles, z_c , is a representative position of the entire layer. Figure 2b shows the temporal evolution of this position for all the simulations, in a semi-logarithmic plot. After the initial transient phase, the curves become linear, meaning that z_c is a logarithmic function of time

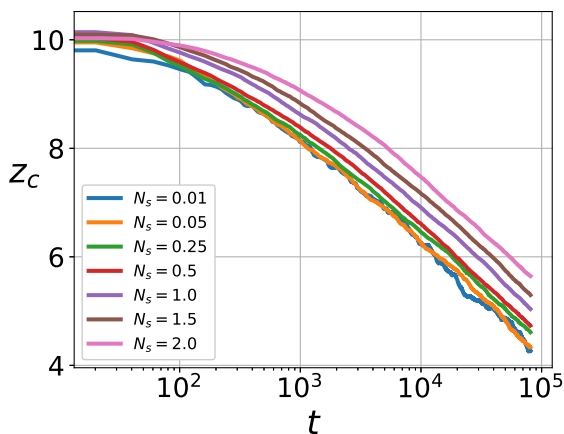
$$z_c = -a \ln(t) + b. \quad (3.3)$$

In equation (3.3), the coefficient a corresponds to the absolute slope of the curve and characterises the segregation velocity ($dz_c/dt = -a/t$). Whatever the number of small particles in the simulation, figure 2b shows that all the curves are parallel to one another, meaning that a is independent of the number of layers of small particles, N_s . Therefore the segregation velocity dz_c/dt is also independent of the number of layers of small particles.

In the following, these simulations will be analysed using the dimensional analysis presented in the introduction (equation (1.4)) with the aim to confirm the dependence of the segregation flux on the inertial number I and on the local concentration ϕ_s .



(a)



(b)

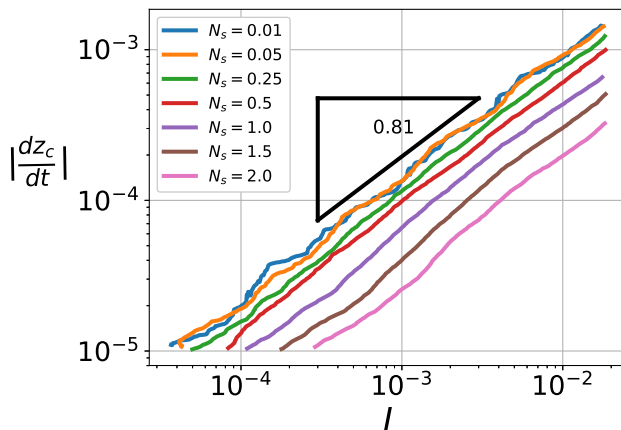
Figure 2: (a) Streamwise space time averaged particle velocity as a function of the height, (b) evolution of the vertical position of the mass center of small particles with time

3.3. Dependence on the inertial number

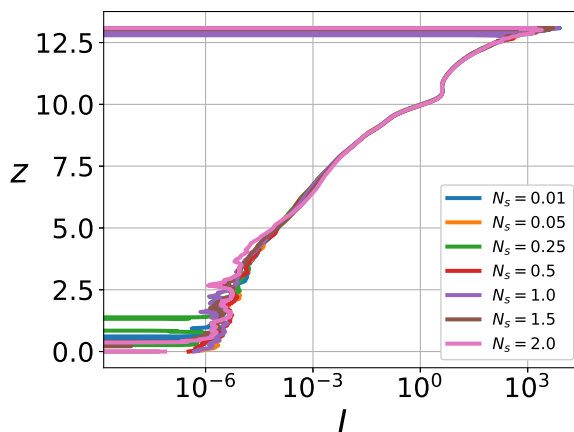
In figure 3a, the dimensionless segregation velocity is plotted against the large particle inertial number $I = \dot{\gamma}^p d_l / \sqrt{P/\rho^p}$. The segregation velocity is higher for larger inertial number. The linearity of the curves shows that the segregation velocity is indeed a power law of the inertial number. For all the simulations the same exponent is obtained and a best fit of the curves gives a value of 0.81 for the exponent,

$$\frac{dz_c}{dt} \propto I^{0.81}. \quad (3.4)$$

Interestingly, Fry *et al.* (2018) obtained a very similar result for dry granular flows at higher inertial numbers ($I \in [10^{-2}, 1]$). They obtained an exponent 0.84, very close to the 0.81 exponent obtained in the present configuration. Our results suggest that the behaviour observed by Fry *et al.* (2018) is valid in a wider range of inertial numbers, in particular, in the quasi-static regime ($I \in [10^{-5}, 10^{-1}]$).



(a)



(b)

Figure 3: (a) Segregation velocity dependence on the local inertial number, (b) inertial number profile

Relation (3.4) allows understanding the temporal evolution of the fine particles center of mass observed previously. Figure 3b shows that the inertial number profile is an exponential function of z as well as $I^{0.81}$ which can be written as

$$I^{0.81} = I_0 e^{z/c}. \quad (3.5)$$

Introducing (3.5) into expression (3.4) leads to

$$\frac{dz_c}{dt} = -b_1 e^{z_c/c}, \quad (3.6)$$

with b_1 a positive constant. Equation (3.6) can be integrated

$$\int e^{-z_c/c} dz_c = \int -b_1 dt, \quad (3.7)$$

N_s	a	c	error (%)
0.01	0.863	0.873	1.159
0.05	0.850	0.864	1.647
0.25	0.823	0.847	2.916
0.5	0.843	0.862	2.254
1	0.833	0.857	2.800
1.5	0.820	0.828	0.976
2	0.849	0.828	2.473

Table 1: Values of coefficients a (slope of the center of mass) and c (exponential decay of the inertial number to the power 0.81) obtained from fitting the curves of figures 2b and 3b and the error in percentage.

leading to

$$ce^{-z_c/c} = b_1 t + Const \sim b_1 t, \quad (3.8)$$

for long times. It can be rewritten as

$$z_c = -c \ln(t) + b_2, \quad (3.9)$$

where $b_2 = -c \ln(b_1/c)$ is a constant. This analysis shows that the logarithmic descent of the small particle center of mass is a consequence of the dependence of the segregation velocity on the inertial number. This is confirmed by the comparison between the coefficients a in equation (3.3) and c in equation (3.5), that should be equal. Fitting of the elevation of the center of mass (figure 2b) and of $I^{0.81}$ yields coefficients a and c (see table 1). The maximal difference between a and c is around 3% confirming the present analysis and showing that the inertial number is indeed the controlling parameter.

3.4. Bottom controlled segregation

While this analysis clearly explains the trends observed, figure 3a shows that for a given value of the inertial number, different segregation velocities are obtained depending on the initial number of small particles, N_s .

Since the inertial number follows an exponential profile, it varies importantly throughout the layer of small particles. Thus according to equation (3.4) the segregation velocity should be lower at the bottom than at the top of the layer. This lower segregation velocity at the bottom of the layer implies that all the small particles above cannot move downward faster than the lowest particles in the layer. Defining the position of the bottom of the layer as $z_b = z_c - W/2$, with $W = 2N_s d_s/d_l$ the small particle layer thickness, figure 4a shows the dependence of the segregation velocity on the inertial number at the bottom of the layer. All the curves collapse on a master curve and a power law relationship is found between the segregation velocity and the inertial number at the bottom of the layer $I_b = I(z_b)$,

$$\frac{dz_c}{dt} = -\alpha_0 I_b^{0.81}, \quad (3.10)$$

where α_0 is a positive constant independent of the number of layers of small particles. This result shows that the segregation velocity of the layer is indeed completely controlled by the inertial number at the bottom of the layer and it does not contain any dependence on the number of small particle layers, N_s .

The layer thickness has been chosen to be two times the thickness it would occupy if

only small particles were present, $W = 2N_s d_s/d_l$. This choice is motivated by the fact that the layer is formed of a mixture of both large and small particles. Figure 4a shows that for the different cases, the width obtained is indeed consistent with the actual thickness. Note that when N_s tends to zero, z_b tends to z_c the center of mass of the small particles. In the extreme case where only one small particle is present, this position corresponds to its center. Figure 4b shows, at time $t = 40435$, the profiles of small particle concentration, where the black crosses denote the position of the bottom of the layer. The lower limb of the concentration profiles are superimposed and the position of the bottom of the layer is identical for all tested values of N_s . Whatever the number of small particles, they pile up above the bottom position, where the segregation dynamics is controlled.

This analysis highlights the dependence of segregation on the inertial number in bedload transport. Furthermore, the bottom of the small particles layer is shown to be a key position that controls segregation. In particular, it explains why the small particles infiltrate the bed as a layer of constant thickness.

3.5. Size ratio influence

The analysis presented above provides a reference position that describes the segregation dynamics. In the following, the effect of the size ratio is investigated. The previous simulations were all performed at the same size ratio, $r = 1.5$. According to the dimensional analysis, the following relationship is expected,

$$\frac{dz_c}{dt} = -\alpha_0(r-1)^l I_b^{0.81}. \quad (3.11)$$

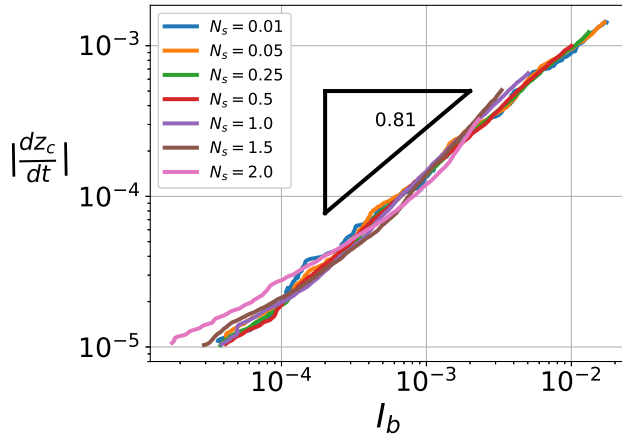
A set of simulations in which the diameter of the small particles is varied was performed with a constant number of small particles layer $N_s = 1$. It covers a range of size ratio from $r = 1.25$ to 2.25 . The dependence of the center of mass velocity on the inertial number at the bottom of the layer of small particles is plotted on figure 5a. A similar power law relationship is recovered (the exponent is slightly larger than previously), showing that the inertial number is still the controlling parameter. The curves are parallel but not superimposed, inducing that, as expected, the size ratio plays an important role in the segregation dynamics. This dependence is presented in figure 5b where the ratio between the segregation velocity and the inertial number to the power 0.81 is plotted as a function of the size ratio minus one. The dimensionless segregation velocity normalised by $I_b^{0.81}$ evolves linearly with $r - 1$ suggesting that the exponent l in (3.11) equals to unity. However the maximal efficiency at $r = 2$ reported by Golick & Daniels (2009), Thornton *et al.* (2012) and Guillard *et al.* (2016) is not recovered in this configuration as the segregation velocity still increases for $r > 2$. This difference with the literature may be due to the fact that segregation is studied here in the quasi-static part of the bed.

To summarize, the results presented herein suggest that the segregation dynamics in bedload transport can be described, at first order, by the following relationship,

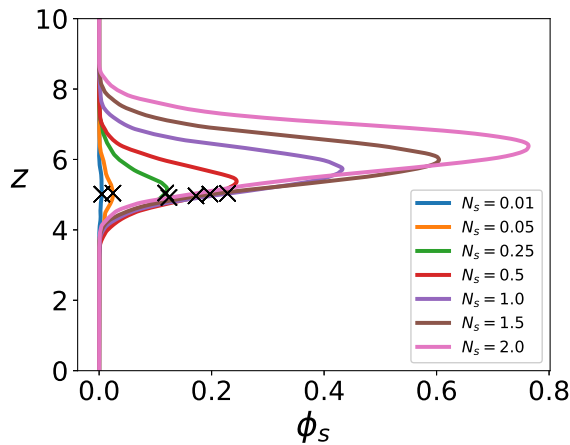
$$\frac{dz_c}{dt} = -\alpha_0(r-1)I_b^{0.81}. \quad (3.12)$$

3.6. Dependence on the local concentration ϕ_s

It is remarkable that the trends observed for the evolution of the center of mass and for the segregation velocity are independent of the number of small particle layers, N_s . Indeed, as the latter is increased from 0.01 to 2, the configuration moves from few isolated (non-interacting) small particles to two consistent layers of small particles infiltrating



(a)



(b)

Figure 4: (a) Center of mass velocity dependence on the inertial number at the bottom of the layer of small particles. (b) Small particles concentration profiles at time $t = 40435$ and vertical position of the bottom of the layer (\times).

collectively inside the coarse bed. Therefore, it is expected that the increase of N_s , would increase the local particle concentration and reduce the segregation velocity due to particle hindrance effects.

This independence of the trend observed in the segregation velocity seems in contradiction with the literature (e.g. Savage & Lun 1988; Dolgunin & Ukolov 1995; Van der Vaart *et al.* 2015; Jones *et al.* 2018), in which a major influence of the local small particle concentration on the segregation velocity has been evidenced. In order to explain this apparent contradiction and get more insight into the physical processes at play, the results are discussed in the following as a function of local mechanisms within the framework of the continuous model of Gray & Thornton (2005), Thornton *et al.* (2006) and Gray & Chugunov (2006).

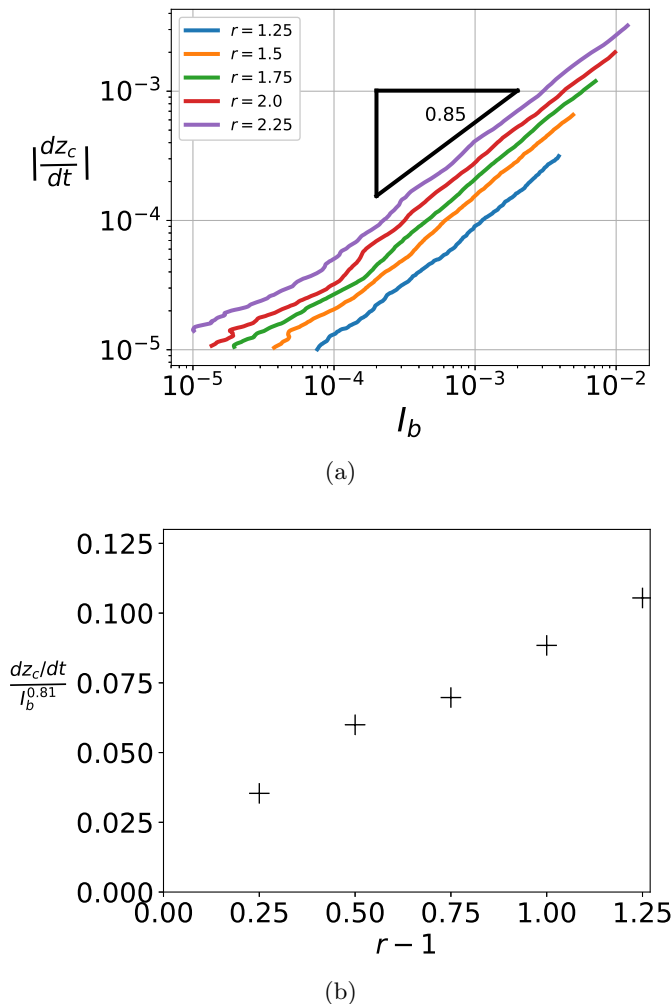


Figure 5: (a): Center of mass velocity dependence on the inertial number at the bottom of the layer of small particles for different size ratio, (b): value of α_0 with the size ratio.

4. Discussion in the framework of continuous modelling

4.1. Local mechanism interpretation

In order to explain the apparent independence of the results on the concentration of small particles, a local analysis in the theoretical framework of continuous modelling is considered. The model of Thornton *et al.* (2006) (1.6), presented in the introduction, will be used as a baseline. In the present configuration, the velocity field has only a streamwise component (along x) and all quantities only depend on z . As a first step, diffusion is not considered and equation (1.6) simplifies to a purely hyperbolic equation,

$$\frac{\partial \phi_s}{\partial t} - \frac{\partial F_s}{\partial z} = 0. \quad (4.1)$$

Combining the form proposed in the introduction, the analysis of the DEM simulations (3.12) and the inertial number functional form (3.5), the segregation flux can be

written as

$$F_s = \alpha_0(r-1)I^{0.81}\phi_s(1-\phi_s) = S_{r0}e^{z/c}\phi_s(1-\phi_s), \quad (4.2)$$

with $S_{r0} = \alpha_0(r-1)I_0$. The inertial number does not depend on the number of small particles (figure 3b) so S_{r0} is independent on the initial number of small particles and only depends on the response of the granular mixture to the fluid flow forcing through I_0 and c . For $r = 1.5$, the corresponding value of S_{r0} obtained from the DEM simulations is: $S_{r0} = 3.70 \times 10^{-8}$. Due to the exponential decrease of the inertial number in the bed, the form of the segregation flux, F_s , is also exponential with z . May *et al.* (2010) already proposed an analytical solution for an exponential flux, but the flow was shear-driven from the bottom. Proceeding similarly, the analytical solution can be derived using the method of characteristics (appendix A) for which the initial condition is simply a step of concentration representing an initial pure layer of small particles lying on a bed made of large particles.

$$\phi_s(z, t = 0) = \begin{cases} 0, & z < z_i, \\ 1, & z \geq z_i, \end{cases} \quad (4.3)$$

with $z_i = N_l d_l$. The solution is plotted in figure 6a for the case $N_s = 1$ and $r = 1.5$. The initial discontinuity leads to an expansion fan delimited by two characteristics (see appendix A). The first, denoted z_1 , is going down and meets the bottom of the domain at time t_1 , which is not reached during the simulations. The second is going up and is denoted z_2 . When it meets the top of the domain at time t_2 (i.e. when the first large particle reaches the top boundary, which happens very rapidly), a shock is created that travels downward. It can be shown (see Appendix A) that the analytical solution for time $t_2 \leq t \leq t_1$ is

$$\phi_s(z, t) = \begin{cases} 0, & z < z_1, \\ \phi_{fan}(z, t), & z_1 \leq z \leq z_2, \\ 0, & z > z_2, \end{cases} \quad (4.4)$$

where z_1 is the characteristic curve (4.5) delimiting the bottom of the rarefaction zone, z_2 is given by the shock equation (4.6) delimiting the top of the rarefaction zone and ϕ_{fan} is the solution in the expansion fan given by (4.7),

$$z_1(t) = z_i - c \ln \left(1 + \frac{S_{r0}}{c} e^{z_i/c t} \right), \quad (4.5)$$

$$\frac{dz_2}{dt} = -S_{r0}e^{z_2/c} (1 - \phi_s(z_2, t)), \quad (4.6)$$

$$\phi_{fan}(z, t) = \frac{1}{2} - \frac{c}{S_{r0}t} e^{-z/c} + \frac{c}{S_{r0}t} e^{-(z+z_i)/(2c)} \sqrt{1 + \left(\frac{S_{r0}t}{2c} \right)^2} e^{(z+z_i)/c}. \quad (4.7)$$

Despite the complexity of the solution (4.4), some simplifications can be made for long times smaller than t_1 . Indeed for long times, the square root term in the second equation of system (4.7) simplifies to

$$1 + \left(\frac{S_{r0}t}{2c} \right)^2 e^{(z+z_i)/c} \sim \left(\frac{S_{r0}t}{2c} \right)^2 e^{(z+z_i)/c}, \quad (4.8)$$

and the volume fraction profile ϕ_s in the rarefaction fan simplifies as,

$$\phi_{fan}(z, t) = 1 - \frac{c}{S_{r0}t} e^{-z/c}. \quad (4.9)$$

Some simplifications can also be done on the boundary curves of the rarefaction zone

z_1 and z_2 . Introducing the long time solution (4.9) in the shock equation of z_2 (4.6), a much more simple equation of z_2 is obtained for long times

$$\frac{dz_2}{dt} = -\frac{c}{t}, \quad (4.10)$$

for which the solution is

$$z_2(t) = -c \ln(t) + \beta, \quad (4.11)$$

where β is an integration constant. Concerning the characteristic curve z_1 , the term in the logarithm in (4.5) simplifies for long times to

$$1 + \frac{S_{r0}}{c} e^{z_i/c} t \sim \frac{S_{r0}}{c} e^{z_i/c} t, \quad (4.12)$$

and the following expression is obtained for z_1

$$z_1(t) = -c \ln(t) - c \ln\left(\frac{S_{r0}}{c}\right). \quad (4.13)$$

Therefore, the upper and lower bounds of the small particle layer, z_2 and z_1 , both move down asymptotically as $-c \ln(t)$, and the layer thickness $z_2(t) - z_1(t)$ is constant. Lastly, the form of the flux considered in the continuum model $F_s \propto I^{0.81} \phi_s (1 - \phi_s)$ implies that the vertical velocity of the small particles $w_s = -F_s / \phi_s$ is

$$w_s(z, t) = -\frac{S_{r0}}{I_0} I^{0.81}(z) (1 - \phi_s(z, t)). \quad (4.14)$$

Using equation (4.9), the vertical velocity can be expressed for long times as

$$w_s(z) = -\frac{S_{r0}}{I_0} I^{0.81} \frac{c}{S_{r0} t} e^{-z/c}, \quad (4.15)$$

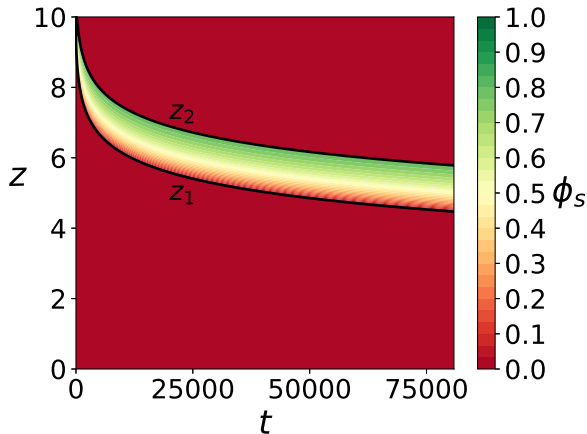
and remembering that $I^{0.81} = I_0 e^{z/c}$,

$$w_s(z) = -\frac{c}{t}. \quad (4.16)$$

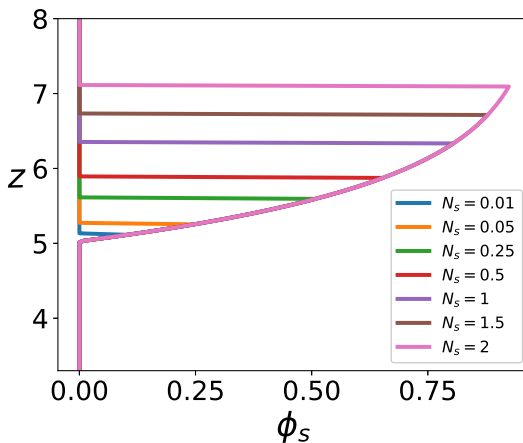
Considering long time solutions and an imposed forcing by the inertial number, the model exhibits the exact same behavior observed in the DEM simulations. First, the small particles move down as a layer into the coarse particles, with the lower and upper bound of the small particles layer showing a logarithmic decrease with time (4.11 and 4.13). This decrease at a common slope $-c$ related to the forcing, imposes a constant layer thickness with time, as observed in the DEM simulations. The consequence is that the segregation velocity of the small particles is the same throughout the layer (4.16). Considering the formulation of the downward velocity of small particles (4.14), this means that the product of the solid volume fraction and the inertial number is constant within the small particle layer,

$$w_s(z, t) = -\frac{S_{r0}}{I_0} I^{0.81}(z) (1 - \phi_s(z, t)) = -c/t. \quad (4.17)$$

Therefore, at a given time, the shape of the small particle concentration profile responds directly to the variation of the inertial number as a function of z . At a point within the layer, the decrease of inertial number observed when going inside the bed is compensated by an increase of the term $1 - \phi_s$, and so a decrease of the solid volume fraction. This competition between the effect of the inertial number and the local concentration results in the shape of solution profiles presented in figure 6b.



(a)



(b)

Figure 6: (a) Case $N_s = 1$, $r = 1.5$ space time evolution of the concentration in fine particles ϕ_s , (b) Profiles of concentration at time $t = 80870$ with the continuum model without diffusion for several values of N_s . The same value of S_r and c have been used.

In order to corroborate the explanation of the mechanisms at play, the lower bound of the small particle layer z_1 for which $\phi_s = 0$ is considered. It corresponds, in figure 6b, to the position where all profiles collapse to zero at the bottom. At this position, the segregation velocity is only a function of the inertial number at the bottom of the layer:

$$w_s(z, t) = -\frac{S_{r0}}{I_0} I^{0.81}(z_1) = -c/t \quad (4.18)$$

This corresponds exactly to the mechanisms evidenced in the DEM simulations in §3.4, where the segregation velocity observed in the simulations have been shown to collapse as a function of the inertial number at a position considered to be the bottom of the small particle layer. The correspondance between the inertial number at the bottom position z_b observed in DEM and the one calculated from the analytical continuum model z_1

N_s	0.01	0.05	0.25	0.5	1	1.5	2
$\frac{ z_1 - z_b }{z_1}$ (%)	0.28	0.22	0.50	0.09	0.04	0.73	0.95

Table 2: Mean error between the bottom position from the DEM simulations z_b and from the continuum model z_1 . The maximal error of less than 1% between both positions suggests that they correspond.

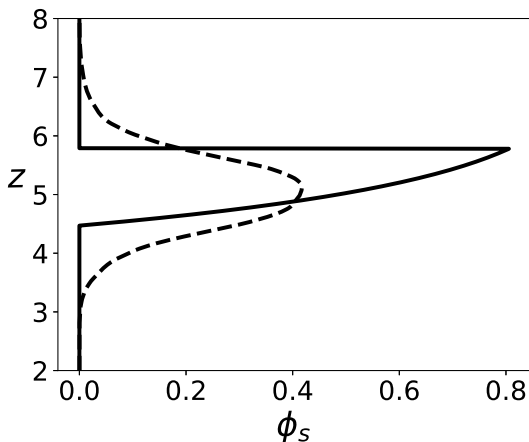


Figure 7: Comparison between DEM simulations (----) and segregation model (—) of the profile of concentration ϕ_s at time $t = 80870$.

(table 2) confirms that the mechanisms evidenced here are indeed the one at play in the DEM simulations.

Finally it is interesting to remark on figure 6b, that all the profiles are going to zero at the exact same position meaning that the bottom position is the same whatever the quantity of small particles. This confirms the DEM result that the segregation velocity is independent of N_s . Indeed, if there are more small particles, they pile up above the others without changing the position of the bottom where the segregation dynamics is controlled.

The continuum model without diffusion enabled understanding of the local segregation mechanisms and gave insights into the underlying physical mechanisms. While this model gives a good agreement at first order, as shown in figure 7, it clearly lacks diffusion in order to reproduce quantitatively the DEM simulations.

4.2. Diffusion and upscaling in a continuous framework

The continuum model used in the previous subsection can be expanded to account for diffusion (Gray & Chugunov 2006), in order to reproduce more quantitatively the DEM results. The equation to be solved is given by,

$$\frac{\partial \phi_s}{\partial t} - \frac{\partial F_s}{\partial z} = \frac{\partial}{\partial z} \left(D \frac{\partial \phi_s}{\partial z} \right), \quad (4.19)$$

with a segregation flux of the form $F_s = S_{r0} e^{z/c} \phi_s (1 - \phi_s)$ and a diffusion coefficient $D(z)$ which is supposed to depend only on the vertical coordinate z . In this paper, a long time

asymptotical solution is presented. At long times, DEM simulations have shown that the shape of the concentration profile ϕ_s is self similar and is only advected downward like a travelling wave. Indeed, the layer of small particles moves down as a layer of constant thickness as $-c \ln(t)$ and the shape of the concentration profile does not evolve with time. The following change of variable is proposed to place the problem in the moving frame of the small particles,

$$\tau = t, \quad \xi = z + c \ln(t). \quad (4.20)$$

Equation (4.19) in the moving frame becomes

$$\frac{\partial \phi_s}{\partial \tau} + \frac{c}{\tau} \frac{\partial \phi_s}{\partial \xi} - \frac{\partial}{\partial \xi} \left(\frac{S_{r0}}{\tau} e^{\xi/c} \phi_s (1 - \phi_s) \right) = \frac{\partial}{\partial \xi} \left(D(\xi - c \ln(\tau)) \frac{\partial \phi_s}{\partial \xi} \right). \quad (4.21)$$

For a travelling wave, the solution to equation (4.21) should not depend on time τ . Assuming $\partial \phi_s / \partial \tau = 0$, this requires that $\tau D(\xi - c \ln(\tau))$ is independent of τ . This implies

$$\frac{\partial}{\partial \tau} (\tau D(\xi - c \ln(\tau))) = 0, \quad (4.22)$$

and distributing the derivative with τ , the following differential equation is obtained

$$D'(\xi - c \ln(\tau)) - \frac{1}{c} D(\xi - c \ln(\tau)) = 0, \quad (4.23)$$

for which the solution is

$$D = D_0 e^{(\xi - c \ln(\tau))/c} = D_0 e^{z/c}. \quad (4.24)$$

This shows that the only way to obtain a time independent solution is that the diffusion coefficient has an exponential structure with the same vertical dependence as the advection flux F_s . In other words, the diffusion coefficient should also be proportional to the inertial number to the power 0.81 in order to have a concentration profile of constant thickness. Under this assumption, equation (4.21) becomes

$$c \frac{\partial \phi_s}{\partial \xi} - \frac{\partial}{\partial \xi} \left(S_{r0} e^{\xi/c} \phi_s (1 - \phi_s) \right) = \frac{\partial}{\partial \xi} \left(D_0 e^{\xi/c} \frac{\partial \phi_s}{\partial \xi} \right). \quad (4.25)$$

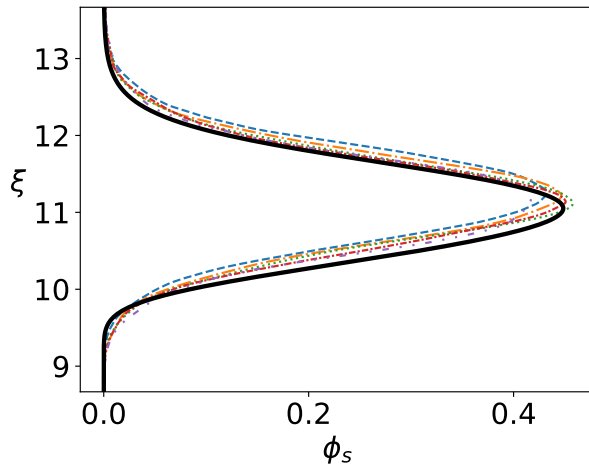
By integration, and imposing $\phi_s \rightarrow 0$ when $\xi \rightarrow \pm\infty$, the following equation is obtained

$$\frac{\partial \phi_s}{\partial \xi} - \frac{S_{r0}}{D_0} \phi_s \left[\phi_s - \left(1 - \frac{c}{S_{r0}} e^{-\xi/c} \right) \right] = 0, \quad (4.26)$$

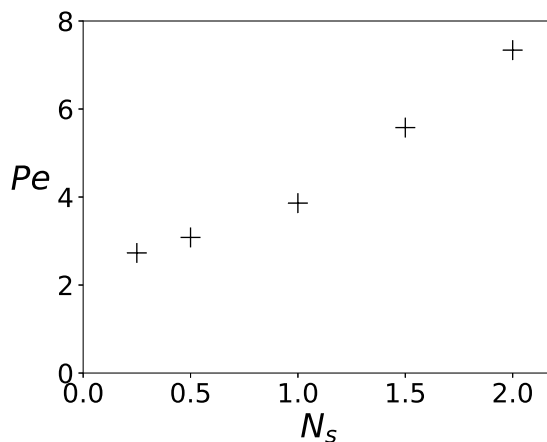
for which the solution is

$$\phi_s = \frac{e^{-\frac{S_{r0}}{D_0} \xi - \frac{c^2}{D_0} e^{-\xi/c}}}{C - \frac{S_{r0}}{D_0} \int_{-\infty}^{\xi} \left(e^{-\frac{S_{r0}}{D_0} \xi' - \frac{c^2}{D_0} e^{-\xi'/c}} \right) d\xi'}, \quad (4.27)$$

where C is a constant satisfying the mass conservation $\int_{-\infty}^{+\infty} \phi_s d\xi$. The travelling wave solution has a complex dependency on ξ and contains an integral which cannot be computed analytically. A semi-analytical approach is developed where the integral is computed numerically and a numerical optimization is performed on the C coefficient so that $\int_{-\infty}^{+\infty} \phi_s d\xi$ corresponds to the initial mass of small particles introduced in the model. Figure 8 compares the travelling wave solution (4.27) with concentration profiles from the DEM simulations (case $N_s = 1$, $r = 1.5$) at different times. The D_0 coefficient was computed in order to minimize the root mean square of the difference between DEM and the travelling wave solution. The travelling wave solution agrees very well with all DEM profiles. The width and the height of the profile are correctly predicted. However



(a)



(b)

Figure 8: (a) Travelling wave solution (—) and concentration profiles in the moving frame from DEM simulations at different times for the case $N_s = 1$, $r = 1.5$, $Pe = 3.86$. $t = 40435$ (---), $t = 50543$ (-.-.-), $t = 60652$ (·····), $t = 70761s$ (-.-.-), $t = 80870$ (-·-·-·-), (b) Value of the Peclet number as a function of the number of layers of small particles.

the latter is slightly below the DEM profiles. This may be explained by the uncertainties when computing the value of S_{r0} from the DEM simulations.

In order to keep the thickness of the small particles layer constant, both the advection and the diffusion coefficients must have the same exponential vertical structure. Defining a Peclet number by the ratio between the segregation intensity and the diffusion coefficient, $Pe = S_r(z)/D(z) = S_{r0}/D_0$, the travelling wave solution leads to a constant Peclet number with depth. The relative effect of segregation and diffusion fluxes is constant and independent of z . At each depth, the balance between advection and diffusion has to be the same in order to be consistent with the constant layer thickness observed in the DEM simulations.

The value of the Peclet number depends on the number of layers of small particles N_s and is plotted in figure 8b. The value of Pe increases almost linearly with N_s . Since the value of S_{r0} is the same whatever the number of layers of small particles, this result suggests that the value of the diffusion coefficient decreases with N_s . This would indicate that diffusion is more efficient when there are fewer small particles. The mean free path of small particles is indeed expected to be larger if they are less concentrated.

This study has shown that both the segregation flux and diffusion need to be proportional to the inertial number to the power 0.81 in order to represent the dynamics of segregation in bedload transport.

5. Conclusion

Vertical size-segregation in bedload transport has been studied with a discrete and a continuous approach. Focusing on the quasi-static region - common to any granular flow on a pile - it has been shown with DEM simulations that small particles infiltrate the coarse quasi-static bed with the same behavior, ranging from a few isolated particles up to two layers of small particles. All the different configurations exhibit the same segregation velocity, related to a power law of the inertial number, generalizing the results observed for moderate inertial numbers in confined granular mixture without fluid (Fry *et al.* 2018). The dynamics of the infiltration of small particles is totally controlled by the bottom of the small particle layer, as the inertial number decreases exponentially from the top to the bottom of the layer. As a consequence, the small particles segregate down as a layer of constant thickness.

The continuous size-segregation model of Gray & Thornton (2005), Thornton *et al.* (2006) and Gray & Chugunov (2006) has been shown to reproduce quantitatively the DEM simulations, with a small particle layer of constant thickness segregating at a velocity independent of the thickness of the layer. In the continuous model, this comes from a perfect balance at any elevation between the effect of the inertial number and the local small particle concentration. This analysis demonstrates that the macroscopic segregation behavior always results from a local equilibrium between the inertial number forcing and the local small particles concentration. Moreover, based on the derivation of an analytical solution with a travelling wave approach, the results show that the diffusion coefficient and the segregation flux in the continuous model should have the same dependency on the inertial number.

This paper represents an original contribution on segregation processes in bedload transport, and more generally in dense granular flows. This is a first step toward upscaling grain size-segregation in continuous models for sediment transport. In the future, it would be interesting to use DEM simulations to infer the different grain-grain forces involved in size-segregation as well as collective effects related to particle concentration.

Acknowledgements

This research was funded by the French Agence nationale de la recherche, project ANR-16-CE01-0005 SegSed 'size segregation in sediment transport'. The authors acknowledge the support of Irstea (formerly Cemagref). This research was supported by NERC grants NE/E003206/1 and NE/K003011/1 as well as EPSRC grants EP/I019189/1, EP/K00428X/1 and EP/M022447/1. J.M.N.T.G. is a Royal Society Wolfson ResearchMerit Award holder (WM150058) and an EPSRC Established Career Fellow (EP/M022447/1).

Appendix A. Solution of the purely advective segregation model

May *et al.* (2010) already derived a solution to the model of Thornton *et al.* (2006) with an exponential dependence of the segregation flux with z . In this appendix, the full solution is presented in the bedload configuration. The segregation equation to solve is:

$$\frac{\partial \phi_s}{\partial t} - \frac{\partial F_s}{\partial z} = 0, \quad (\text{A } 1)$$

with the flux $F_s = S_{r0} e^{z/c} \phi_s (1 - \phi_s)$ and an initial step condition in concentration:

$$\phi_{s0} = \phi_s(z, 0) = \begin{cases} 0, & z < z_i, \\ 1, & z \geq z_i. \end{cases} \quad (\text{A } 2)$$

The boundary conditions ensure that there is no flux at $z = 0, H$, which requires that

$$\phi_s = 0 \text{ or } 1, \quad \text{at } z = 0 \text{ and } H. \quad (\text{A } 3)$$

Substituting the flux into (A 1) implies

$$\frac{\partial \phi_s}{\partial t} + W(z, \phi_s) \frac{\partial \phi_s}{\partial z} = S(z, \phi_s) \quad (\text{A } 4)$$

where

$$W(z, \phi_s) = S_{r0} e^{z/c} (2\phi_s - 1), \quad (\text{A } 5)$$

$$S(z, \phi_s) = \frac{S_{r0}}{c} e^{z/c} \phi_s (1 - \phi_s). \quad (\text{A } 6)$$

Due to dependence of the flux both on z and ϕ_s , the equation to solve has a non-linear advective velocity and a source term. In the following, this problem is solved using the method of characteristics.

On a characteristic curve $(Z(s), t(s))$,

$$\frac{d\phi_s}{ds} = \frac{\partial \phi_s}{\partial t} \frac{dt}{ds} + \frac{\partial \phi_s}{\partial z} \frac{dz}{ds} = S. \quad (\text{A } 7)$$

Comparing coefficients of (A 4) and (A 7)

$$\frac{d\phi_s}{ds} = S, \quad (\text{A } 8)$$

$$\frac{dt}{ds} = 1, \quad (\text{A } 9)$$

$$\frac{dZ}{ds} = W. \quad (\text{A } 10)$$

Eliminating s implies

$$\frac{d\phi_s}{dt} = S \quad (\text{A } 11)$$

$$\frac{dZ}{dt} = W. \quad (\text{A } 12)$$

The problem (A 4) is thus equivalent to the following system:

$$\left\{ \begin{array}{l} \frac{d}{dt} \phi_s(Z(t), t) = S(Z(t), \phi_s(Z(t), t)), \\ \frac{dZ(t)}{dt} = W(Z(t), \phi_s(Z(t), t)), \\ Z(0) = z_0. \end{array} \right. \quad (\text{A } 13)$$

The first equation indicates that ϕ_s is not constant along a characteristic curve and the second equation that the characteristic curves are not linear. The method of characteristics consists in solving the value of ϕ_s along the characteristics curves. If a characteristic curve passing by each time and space position exists, then the problem can be fully resolved. In order to compute the value of ϕ_s along a characteristic curve, the first equation of (A 13) is differentiated with time

$$\frac{d^2}{dt^2} \phi_s(Z(t), t) = \frac{d}{dt} [S(Z(t), \phi_s(Z(t), t))], \quad (\text{A } 14)$$

distributing the derivative,

$$\frac{d^2}{dt^2} \phi_s(Z(t), t) = \frac{dZ}{dt} \frac{\partial S}{\partial z} + \frac{d\phi_s(Z(t), t)}{dt} \frac{\partial S}{\partial \phi_s}, \quad (\text{A } 15)$$

and introducing the first and second equation of (A 13) it implies,

$$\frac{d^2}{dt^2} \phi_s(Z(t), t) = W \frac{\partial S}{\partial z} + S \frac{\partial S}{\partial \phi_s}. \quad (\text{A } 16)$$

Using equation (A 5) and (A 6), one can remark that $\partial S/\partial z = S/c$ and $\partial S/\partial \phi_s = -W/c$. Introducing this in (A 16), the second derivation with time of ϕ_s along a characteristic curve is identically null,

$$\frac{d^2}{dt^2} \phi_s(Z(t), t) = 0. \quad (\text{A } 17)$$

Integrating twice with time, a linear dependence on time of ϕ_s is obtained,

$$\phi_s(Z(t), t) = \phi_{s0}(z_0) + S(z_0, \phi_{s0}(z_0)) t. \quad (\text{A } 18)$$

The value of ϕ_s along the characteristic curve is entirely determined by its initial value and therefore by the initial condition ϕ_{s0} . It is now possible to compute the position with time of a characteristic curve. Introducing (A 18) in the second equation of (A 13) and integrating, a relation for the characteristic curves is obtained,

$$e^{-Z(t)/c} - e^{-z_0/c} = -\frac{S_{r0}}{c} (2\phi_{s0}(z_0) - 1)t - \frac{S_{r0}}{c} S(z_0, \phi_{s0}(z_0)) t^2, \quad (\text{A } 19)$$

$$\Leftrightarrow Z(t) = z_0 - c \ln \left(1 - \frac{1}{c} W(z_0, \phi_{s0}(z_0)) t - \frac{S_{r0}}{c} e^{z_0/c} S(z_0, \phi_{s0}(z_0)) t^2 \right), \quad (\text{A } 20)$$

and the characteristic curve is entirely determined by the value of the initial solution ϕ_{s0} in its origin position z_0 . Finally the solution to system (A 13) is

$$\left\{ \begin{array}{l} \phi_s(Z(t), t) = \phi_{s0}(z_0) + S(z_0, \phi_{s0}(z_0)) t, \\ Z(t) = z_0 - c \ln \left(1 - \frac{1}{c} W(z_0, \phi_{s0}(z_0)) t - \frac{S_{r0}}{c} e^{z_0/c} S(z_0, \phi_{s0}(z_0)) t^2 \right), \end{array} \right. \quad (\text{A } 21)$$

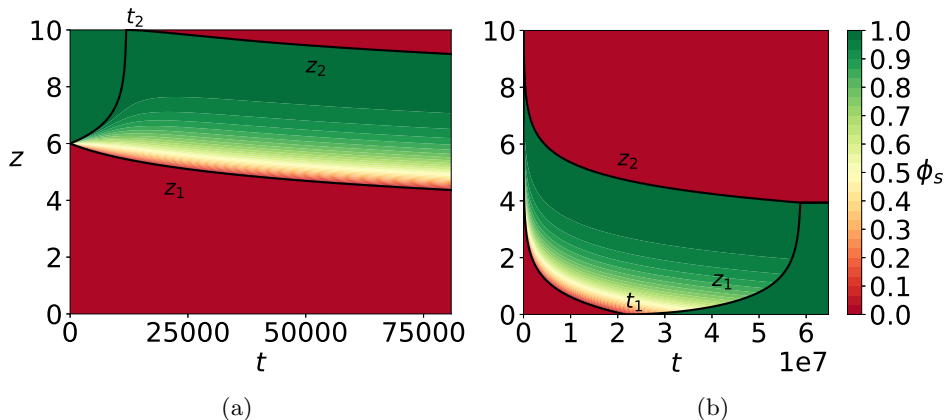


Figure 9: Example of solution obtained by the method of characteristics. $z_i = 6$ (a) First time steps, (b) full solution.

Equation (A 21) is a general solution for any initial condition. In the present configuration the initial solution (A 2) is a step of concentration with a discontinuity at z_i and represents an initial state where a pure layer of small particles is placed above a bed of only large particles. Figure 9 shows the full solution for the case $z_i = 6$, and the derivation of this solution is presented below. According to the second equation of (A 13), the characteristic curves coming from $z_0 < z_i$ have a negative velocity and are going down. Conversely, those coming from $z_0 > z_i$ are going up. Therefore there is a rarefaction fan, where no characteristic curves are present.

For $z_0 < z_i$, $\phi_{s0}(z_0) = 0$, the equation of the characteristic curves are $Z(t) = z_0 - c \ln(1 + \frac{S_{r0}}{c} e^{z_0/ct})$. Along these characteristics, $\phi_s(Z(t), t) = 0$. z_1 is defined as the characteristic curve at the bottom of the rarefaction zone (coming from z_i): $z_1(t) = z_i - c \ln(1 + \frac{S_{r0}}{c} e^{z_i/ct})$. z_1 is the lower bound of the rarefaction zone. The time at which z_1 meets the bottom of the domain is called $t_1 = \frac{c}{S_{r0}}(1 - e^{-z_i/c})$ and corresponds to the time when the first small particle reaches the bottom.

For $z_0 > z_i$, $\phi_{s0}(z_0) = 1$, the equation of the characteristic curves are $Z(t) = z_0 - c \ln(1 - \frac{S_{r0}}{c} e^{z_0/ct})$. Along these characteristics, $\phi_s(Z(t), t) = 1$. z_2 is defined as the characteristic curve coming from z_i : $z_2(t) = z_i - c \ln(1 - \frac{S_{r0}}{c} e^{z_i/ct})$. z_2 is the upper bound of the rarefaction zone. The time at which z_2 meets the top of the domain is called $t_2 = \frac{c}{S_{r0}}(e^{-z_i/c} - e^{-H/c})$ and corresponds to the time when the first large particle reaches the top.

Once z_2 reaches the top of domain at t_2 the boundary condition (A 3) implies that $\phi(H, t_2)$ jumps from 1 to 0. A shock forms and the position of the shock must satisfy the Rankine-Hugoniot relation, which ensures the conservation of momentum through the shock :

$$z_2' = -\frac{F_s(\phi^+) - F_s(\phi^-)}{\phi^+ - \phi^-}.$$

Above the shock $\phi^+ = 0$ and below ϕ^- is the solution in the rarefaction zone:

$$z_2' = -S_{r0} e^{z_2/c} (1 - \phi_s(z_2, t)). \quad (\text{A } 22)$$

A similar expression applying the Rankine-Hugoniot relation is found for z_1 for $t > t_1$. For now, as no solution in the rarefaction has been computed, the shock evolution equation (A 22) cannot be solved. The solution in the rarefaction zone is now computed.

The rarefaction zone is delimited by z_1 and z_2 . Due to the discontinuity in the initial solution, no characteristic curves are present in the rarefaction wave ($z_1 \leq z \leq z_2$). In order to find a solution, it is considered that there is an infinity of characteristic curves coming from the point of discontinuity z_i , each of them being associated to a different initial value, noted $\bar{\phi}_{s0}$ and verifying $\phi_{s0}(z_c)^- = 0 \leq \bar{\phi}_{s0} \leq 1 = \phi_{s0}(z_c)^+$. In other words, for (z, t) in the rarefaction zone, one looks for a characteristic curve coming from z_i associated to an initial value $\bar{\phi}_{s0}$ and verifying system (A 21):

$$\begin{cases} \phi_s(z, t) &= \bar{\phi}_{s0} + S(z_i, \bar{\phi}_{s0}) t, \\ e^{-z/c} - e^{-z_i/c} &= -\frac{S_{r0}}{c}(2\bar{\phi}_{s0} - 1)t - \frac{S_{r0}}{c} e^{z_i/c} S(z_i, \bar{\phi}_{s0}) t^2. \end{cases} \quad (\text{A } 23)$$

To compute the value of ϕ_s in the rarefaction zone with the first equation of (A 23), only the value of $\bar{\phi}_{s0}$ is missing. It is computed by an inversion of the second equation of (A 23) (quadratic equation and choosing the relevant solution):

$$\bar{\phi}_{s0} = \frac{1}{2} + \frac{c}{S_{r0}t} e^{-z_i/c} \left(1 - e^{(z_i-z)/c} \sqrt{1 + \left(\frac{S_{r0}t}{2c} \right)^2 e^{(z+z_i)/c}} \right). \quad (\text{A } 24)$$

Inserting (A 24) into the first equation of (A 23) the solution in the rarefaction zone is:

$$\phi_s(z, t) = \frac{1}{2} - \frac{c}{S_{r0}t} e^{-z/c} + \frac{c}{S_{r0}t} e^{-(z+z_i)/(2c)} \sqrt{1 + \left(\frac{S_{r0}t}{2c} \right)^2 e^{(z+z_i)/c}}. \quad (\text{A } 25)$$

The equation of the shock (A 22) can now be solved. However due to the complex form of the solution in the rarefaction zone (A 25) the equation of the shock (A 22) is solved numerically. Finally the full solution is presented on figure 9.

REFERENCES

- BATHURST, J.C. 2007 Effect of Coarse Surface Layer on Bed-Load Transport. *Journal of Hydraulic Engineering* **133** (11), 1192–1205.
- BRIDGWATER, J., FOO, W.S. & STEPHENS, D.J. 1985 Particle mixing and segregation in failure zones—theory and experiment. *Powder Technology* **41** (2), 147–158.
- BRIDGWATER, J. & INGRAM, N.D. 1971 Rate of Spontaneous Inter-Particle Percolation. *Transactions of the Institution of Chemical Engineers* **49** (3), 163–169.
- CAMPBELL, C. S. 1997 Self-diffusion in granular shear flows. *Journal of Fluid Mechanics* **348**, 85–101.
- CHAUCHAT, J. 2018 A comprehensive two-phase flow model for unidirectional sheet-flows. *Journal of Hydraulic Research* **56** (1), 15–28.
- DOLGUNIN, V. N. & UKOLOV, A. A. 1995 Segregation modeling of particle rapid gravity flow. *Powder Technology* **83** (2), 95–103.
- DUDILL, A., FREY, P. & CHURCH, M. 2017 Infiltration of fine sediment into a coarse mobile bed: A phenomenological study. *Earth Surface Processes and Landforms* **42** (8), 1171–1185.
- DUDILL, A., LAFAYE DE MICHEAUX, H., FREY, P. & CHURCH, M. 2018 Introducing Finer Grains Into Bedload: The Transition to a New Equilibrium. *Journal of Geophysical Research: Earth Surface* **123** (10), 2602–2619.
- FAN, Y., SCHLICK, C. P., UMBANHOWAR, P. B., OTTINO, J. M. & LUEPTOW, R. M. 2014 Modelling size segregation of granular materials: The roles of segregation, advection and diffusion. *Journal of Fluid Mechanics* **741**, 252–279.
- FERDOWSI, B., ORTIZ, C. P., HOUSSAIS, M. & JEROLMACK, D. J. 2017 River-bed armouring as a granular segregation phenomenon. *Nature Communications* **8** (1).
- FREY, P. 2014 Particle velocity and concentration profiles in bedload experiments on a steep slope. *Earth Surface Processes and Landforms* **39** (5), 646–655.

- FREY, P. & CHURCH, M. 2011 Bedload: A granular phenomenon. *Earth Surface Processes and Landforms* **36** (1), 58–69.
- FRY, A. M., UMBANHOWAR, P. B., OTTINO, J. M. & LUEPTOW, R. M. 2018 Effect of pressure on segregation in granular shear flows. *Physical Review E* **97** (6-1), 062906.
- GAJJAR, P. & GRAY, J. M. N. T. 2014 Asymmetric flux models for particle-size segregation in granular avalanches. *Journal of Fluid Mechanics* **757**, 297–329.
- GDR MiDi 2004 On dense granular flows. *The European Physical Journal E* **14** (4), 341–365.
- GOLICK, L. A. & DANIELS, K. E. 2009 Mixing and segregation rates in sheared granular materials. *Physical Review E* **80** (4), 042301.
- GRAY, J.M.N.T & THORNTON, A.R 2005 A theory for particle size segregation in shallow granular free-surface flows. *Proceedings of the Royal Society A: Mathematical, Physical and Engineering Sciences* **461** (2057), 1447–1473.
- GRAY, J. M. N. T. & ANCEY, C. 2011 Multi-component particle-size segregation in shallow granular avalanches. *Journal of Fluid Mechanics* **678**, 535–588.
- GRAY, J. M. N. T. & CHUGUNOV, V. A. 2006 Particle-size segregation and diffusive remixing in shallow granular avalanches. *Journal of Fluid Mechanics* **569**, 365–398.
- GUILLARD, F., FORTERRE, Y. & POULIQUEN, O. 2016 Scaling laws for segregation forces in dense sheared granular flows. *Journal of Fluid Mechanics* **807**.
- HERGAULT, VIRGINIE, FREY, PHILIPPE, MÉTIVIER, FRANÇOIS, BARAT, CÉCILE, DUCOTTET, CHRISTOPHE, BÖHM, TOBIAS & ANCEY, CHRISTOPHE 2010 Image processing for the study of bedload transport of two-size spherical particles in a supercritical flow. *Experiments in Fluids* **49** (5), 1095–1107.
- JACKSON, R. 2000 *The Dynamics of Fluidized Particles*. Cambridge University Press.
- JONES, R. P., ISNER, A. B., XIAO, H., OTTINO, J. M., UMBANHOWAR, P. B. & LUEPTOW, R. M. 2018 Asymmetric concentration dependence of segregation fluxes in granular flows. *Physical Review Fluids* **3** (9).
- LI, L. & SAWAMOTO, M. 1995 Multi-Phase Model on Sediment Transport in Sheet-Flow Regime Under Oscillatory Flow. *Coastal Engineering in Japan* **38** (2), 157–178.
- MAURIN, R., CHAUCHAT, J., CHAREYRE, B. & FREY, P. 2015 A minimal coupled fluid-discrete element model for bedload transport. *Physics of Fluids* **27** (11), 113302.
- MAURIN, R., CHAUCHAT, J. & FREY, P. 2016 Dense granular flow rheology in turbulent bedload transport. *Journal of Fluid Mechanics* **804**, 490–512.
- MAY, L. B. H., GOLICK, L. A., PHILLIPS, K. C., SHEARER, M. & DANIELS, K. E. 2010 Shear-driven size segregation of granular materials: Modeling and experiment. *Physical Review E* **81** (5), 051301.
- MIDDLETON, G. V. 1970 Experimental studies related to problems of flysch sedimentation.
- RICHARDSON, J. F. & ZAKI, W. N. 1954 The sedimentation of a suspension of uniform spheres under conditions of viscous flow. *Chemical Engineering Science* **3** (2), 65–73.
- ROUX, J.N. & COMBE, G. 2002 Quasistatic rheology and the origins of strain. *Comptes Rendus Physique* **3** (2), 131–140.
- SAVAGE, S. B. & LUN, C. K. K. 1988 Particle size segregation in inclined chute flow of dry cohesionless granular solids. *Journal of Fluid Mechanics* **189**, 311–335.
- SCHWAGER, T. & POSCHEL, T. 2007 Coefficient of restitution and linear-dashpot model revisited. *Granular Matter* **9** (6), 465–469.
- SMILAUER ET AL., V. 2015 *Yade Documentation 2nd Ed. The Yade Project..* Zenodo, 10.5281/zenodo.34073.
- THORNTON, A., WEINHART, T., LUDING, S. & BOKHOVE, O. 2012 Modeling of particle size segregation: Calibration using discrete particle method. *International Journal of Modern Physics C* **23** (08), 1240014.
- THORNTON, A. R., GRAY, J. M. N. T. & HOGG, A. J. 2006 A three-phase mixture theory for particle size segregation in shallow granular free-surface flows. *Journal of Fluid Mechanics* **550**, 1–25.
- UTTER, B. & BEHRINGER, R. P. 2004 Self-diffusion in dense granular shear flows. *Physical Review E* **69** (3), 031308.
- VAN DER VAART, K., GAJJAR, P., EPELY-CHAUVIN, G., ANDREINI, N., GRAY, J. & ANCEY, C. 2015 Underlying Asymmetry within Particle Size Segregation. *Physical review letters* **114**.

WIEDERSEINER, S., ANDREINI, N., EPELY-CHAUVIN, G., MOSER, G., MONNEREAU, M. L., GRAY, J. M. & ANCEY, C. 2011 Experimental investigation into segregating granular flows down chutes.